Investigation on the shockwave induced by surface arc plasma in quiescent air*

Jin Di(金 迪)†, Li Ying-Hong(李应红), Jia Min(贾 敏), Li Fan-Yu(李凡玉), Cui Wei(崔 巍), Sun Quan(孙 权), Zhang Bai-Ling(张百灵), and Li Jun(李 军)

Science and Technology on Plasma Dynamics Laboratory, Air Force Engineering University, Xi'an 710038, *China*

(Received 17 July 2013; revised manuscript received 3 September 2013; published online 24 January 2014)

The shockwave induced by surface direct-current (DC) arc discharge is investigated both experimentally and numerically. In the experiment, the shockwave generated by rapid gas heating is clearly observed from Schlieren images. The peak velocity of the shockwave is measured to be over 410 m/s; during its upright movement, it gradually falls to about 340 m/s; no remarkable difference is seen after changing the discharge voltage and the pulse frequency. In the modeling of the arc plasma, the arc domain is not simulated as a boundary condition with fixed temperature or pressure, but a source term with a time-varying input power density, which could better reflect the influence of the heating process. It is found that with a reference power density of 2.8×10^{12} W/m^3, the calculated peak velocity is higher than the measured one, but they quickly (in 30 μs) become agreed with each other. The peak velocity also rises while increasing the power density, the maximum velocity acquired in the simulation is over 468 m/s, which is expected to be effective for high speed flow control.

Keywords: surface arc, pulsed DC discharge, shockwave, propagation velocity

PACS: 52.50.Nr, 52.80.Mg, 47.80.Jk **DOI:** 10.1088/1674-1056/23/3/035201

1. Introduction

The plasma aerodynamic actuator has drawn increasing attention worldwide for its potential applications in both low and high speed flow controls.[1,2] There are three widely accepted mechanisms of plasma flow control, which could be listed as follows: (i) electrohydrodynamics (EHD) forcing driven by the momentum transfer between neutral background gas molecules and charged particles drifting in an electric field, (ii) magnetohydrodynamics (MHD) forcing achieved when an external magnetic field is applied to the charged particles and creates a Lorentz force, (iii) localized gas heating that creates a fast and strong disturbance or a virtual shape to change the flow structure. The dominating mechanism may be varied for different plasma sources or actuators. It is generally believed that in a low speed flow, the electrostatic force plays an important role, while in a supersonic flow, the heating mechanism may be more convincing.[3,4]

Leonov *et al.* discussed the mechanisms of flow control through near-surface electrical discharge. The shockwave structure modification, separation control, mixing intensification, and plasma-assisted combustion/ignition by arc discharge were also researched.[5–9] Samimy *et al.* investigated the control of high-speed high-Reynolds-number jets through localized arc filament plasmas. The best control of jet potential core length and centerline velocity distribution was acquired with a Strouhal number of 0.33 and azimuthal mode $m = \pm1$.[10,11] Shneider *et al.* proposed the concept of hypersonic aerodynamic control and thrust vectoring through MHD devices, the power needed for a plasma-related process was planned to be generated through an MHD power extraction.[12,13] In the research of Shang, the plasma induced compression was achieved at the entrance of rectangular and cylindrical cross section models in Mach 5 flows.[14,15] Kuo *et al.* developed a portable arc microwave plasma torch aiming at the assisted ignition in a supersonic combustor. Besides, wind tunnel experiments were conducted to explore the modification effects of plasma spikes on the shockwave structure in front of a 60° cone.[16,17] Ni *et al.* investigated a novel water plasma torch, a high thermal efficiency was confirmed analytically and experimentally.[18] The arc-root attachment on the anode surface of a direct-current (DC) arc plasma torch was observed by Pan *et al.*, it was also found that the constricted arc roots often occurred when hydrogen or nitrogen was added in the working gas.[19] Xu *et al.* experimentally investigated the hydrodynamic expansion after a nanosecond repetitively pulsed discharge in atmospheric air preheated up to 1000 K, the velocity of the induced pressure wave was expected to be the sound speed, both temperature and pressure behind the shock front were calculated and discussed under different electrode distances, different pulse repetition frequencies, and different air temperatures. The presented results confirmed the ultrafast heating mechanism of such discharge.[20] By a numerical simulation, Gaitonde *et al.* researched the control effect of a localized arc filament plasma actuation on a Mach 1.3 supersonic jet. A three-dimensional simulation was also carried out

*Project supported by the Key Program of the National Natural Science Foundation of China (Grant No. 51336011) and the National Natural Science Foundation of China (Grant Nos. 51207169 and 51276197).

†Corresponding author. E-mail: james.8653@gmail.com

© 2014 Chinese Physical Society and IOP Publishing Ltd

to explore the influence of a pulsed surface thermal bump on a Mach 1.5 flat plate laminar boundary layer.[21,22]

In this paper, the shockwave induced by pulsed arc discharge on a flat ceramic plate is experimentally and numerically studied. A shockwave induced by fast heating is observed. According to Schlieren images, the development of the shockwave and its transmitting speed are specified. In the numerical simulation, instead of taking the arc filament as a boundary condition with fixed temperature or pressure, the input power density is added as a source term for the purpose of describing the real heating process. After being validated by experiments, simulations are designed to show the influence of the discharge power density on the shockwave movement.

2. Experimental investigation

2.1. Experimental setup

The experiment is conducted in the atmospheric air with a temperature of about 300 K. A pulsed-DC power supply is adopted, the output voltage ranges from 0 kV to 20 kV, and the repetition frequency varies from 100 Hz to 2000 Hz. The pulse voltage applied on the electrodes is measured with a high voltage probe (P6015A, Tektronix), while the discharge current is measured and amplified with a current probe (TCP312, Tektronix) and an amplifier (TCPA300, Tektronix). These two signals are displayed and recorded through an oscilloscope (DPO4140, Tektronix). The arc discharge actuator consists of a pair of round tungsten electrodes and a dielectric ceramic plate made of aluminum oxide. Two 10-mm-diameter electrodes are smoothly mounted into the ceramic plate, considering the capability of the power supply, the gap of the electrodes is set to be 6 mm.

A Schlieren system is designed for the flow visualization, by which the density variation of the fluid field can be shown. A Phantom V310 high speed camera is used to capture the images, which is operated with a framing rate of 22012 Hz (frame interval of 45.43 μs) and an exposure time of 1.02 μs. The images (240×400 pixel resolution) can be recorded for 7.5 s. The camera is triggered by a Stanford Research System DG535 delay/pulse generator. When the discharge initiates and is detected by the TCP312 current probe, a signal will be generated and transmitted from the oscilloscope to the DG535 delay/pulse generator, then the DG535 generator outputs a level signal to start the camera with a preset delay. At each discharge experiment, the responding time from breakdown to camera starting is fixed through adjusting the delay time of DG535, then the time resolved Schlieren measurement can be realized. The schematic diagram of experiment setup and plasma actuator is shown in Fig. 1.

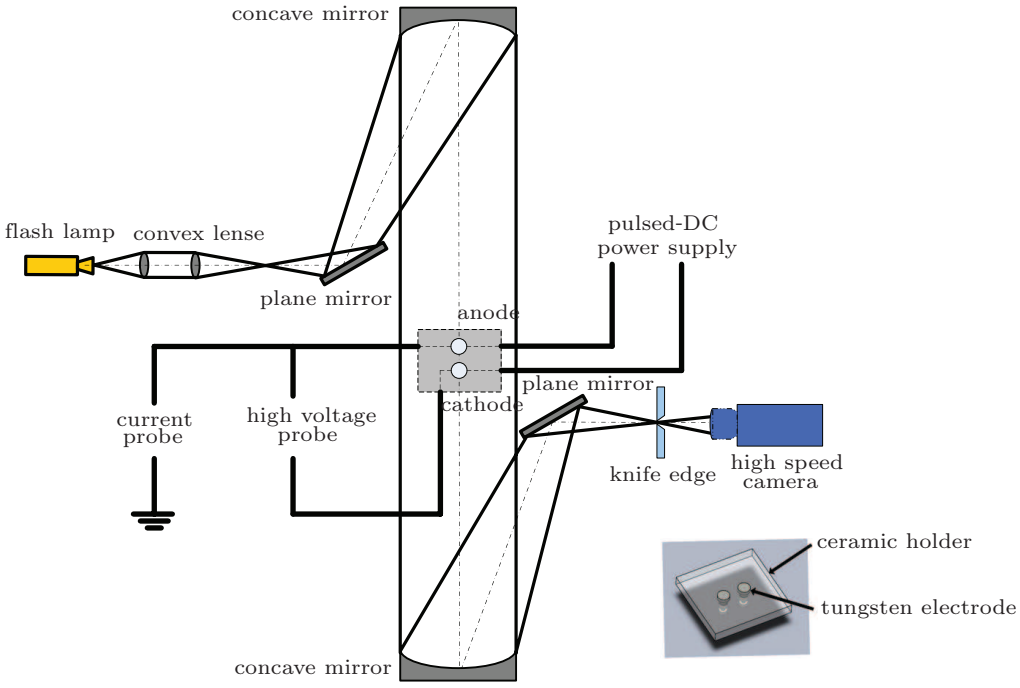


Fig. 1. (color online) Schematic diagram of experiment setup and plasma actuator (inset).

2.2. Experiment results

2.2.1. Electrical characteristics

Figure 2 shows the plots of voltage and discharge current during a single pulse. The pulse frequency and the discharge voltage are 1 kHz and 15.7 kV, respectively. As soon as the circuit is switched on, the air between the electrodes will be broken down and arc plasma will be created. The power supply is designed to output a negative pulse. Based on the *V*–*I*

characteristic of the arc discharge, the voltage will decrease after discharge is generated, so the voltage increases sharply from about −15.7 kV to 0 kV within 200 ns. Here the high absolute value of the discharge voltage is determined by the gap between the electrodes, the output voltage must exceed the breakdown voltage to ensure the discharge. The current increases dramatically nearly 40 A within 600 ns and gradually falls back, the duration of a single pulse lasts about 6 μs.

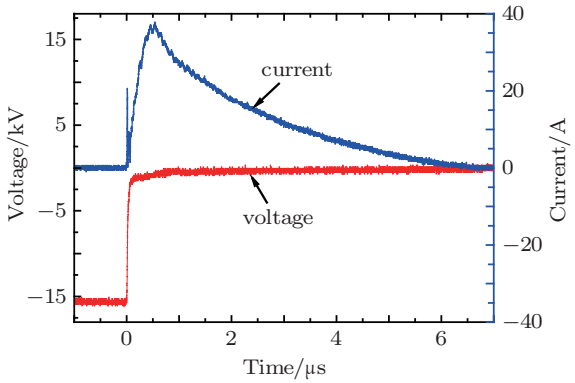


Fig. 2. (color online) The *V*–*I* plot with discharge frequency of 1 kHz and voltage of 15 kV.

At a high sample rate of 1 GHz, when a negative pulse is applied and discharge is initiated, an obvious spike can be observed (the spike can be easily missed under a lower sample rate). That is to say, the discharge with a lower current and a short duration occurs when the voltage begins to rise, and then the arc filament is established. Such spikes are detected in all the experiments, excluding the possibility of EM noise or imperfect contact.

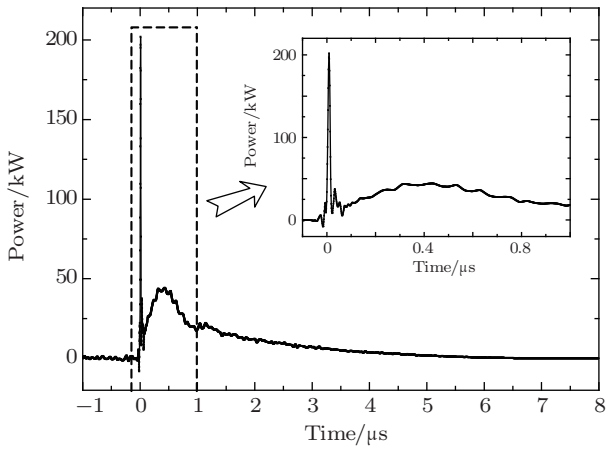


Fig. 3. Instantaneous power plot with discharge frequency of 1 kHz and voltage of 15 kV, an enlarged view is shown in the inset.

Figure 3 shows the instantaneous discharge power according to the *V*–*I* plot in Fig. 2. The voltage and the current are multiplied to represent the energy deposited into the arc channel at each sampling moment. There is a very high peak value over 200 kW at the beginning of discharge, which corresponds to the current spike. Although the subsequent current is larger than the spike, the voltage is only about 100–300 V, the power is still lower than 50 kW. After a wave crest about 45 kW at 450 ns, the instantaneous power slowly drops to zero in the next 5 μs.

2.2.2. Morphology of arc plasma

The images of arc plasma are shown in Fig. 4, three independent pulses are chosen to describe the morphological character. From Fig. 4(a), it is easy to find that at all discharges, quite bright blue-violet filaments are created between the electrodes, which demonstrate the typical formation of arc plasma. Meanwhile, the path of breakdown and the shape of the arc channel vary obviously from one discharge to another. Contrary to the theoretical prediction, the breakdowns do not always occur in the shortest gap, the breakdown paths are totally random. Figure 4(b) shows the upright movement of arc plasma after being generated. Keeping the experiment setup unchanged, the shapes of arc plasma in the three pulses are different. Once an arc filament is created, the air around it will be drastically heated and forms a high temperature and pressure block, from which the shockwave is originated.

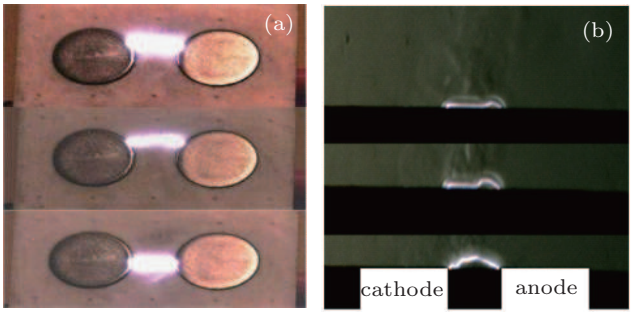


Fig. 4. (color online) Images of arc discharge: (a) top view, (b) side view.

2.2.3. Propagation of arc induced shockwave

Through the Schlieren system, the time resolved images of the arc induced shockwave are acquired. At first, the smallest delay time is set to be as short as 1 μs. During this delay, the shockwave is estimated to move only about 0.4 mm, which is quite difficult to be measured accurately. So the delay time is chosen to be 5 μs or 10 μs. The moment at which the breakdown occurs is taken as the time zero point, the time interval between the first 9 images is 5 μs, for the other images, the time delay is 10 μs. Images in Fig. 5 show that only several microseconds after the air has been heated, a shockwave is induced by the sharp rise of temperature and pressure, the inside temperature of the heat block is believed to reach 1000 K.

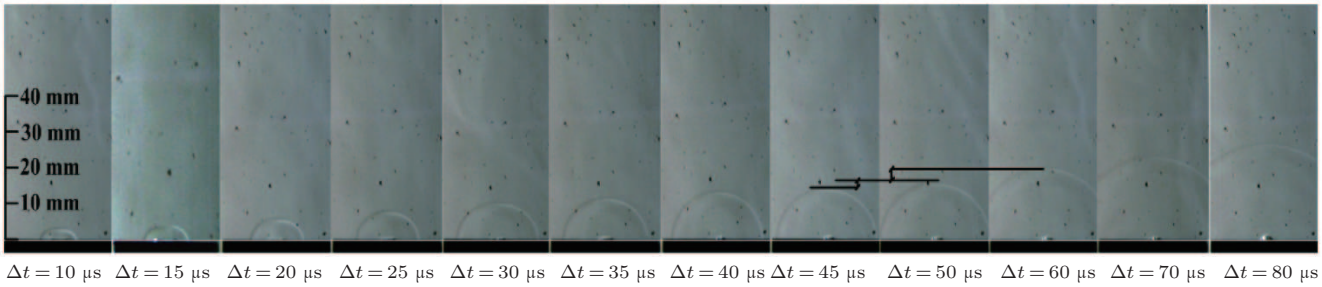


Fig. 5. (color online) Propagation of arc induced shockwave into quiescent air.

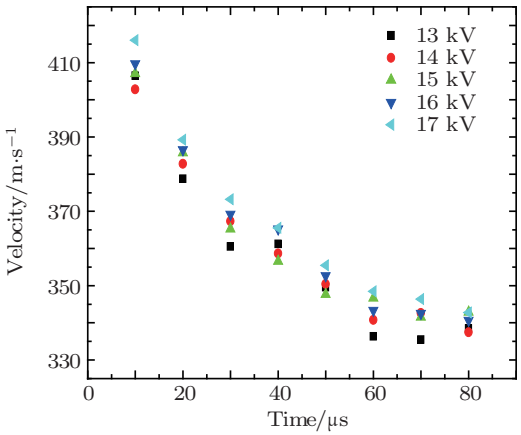


Fig. 6. (color online) Velocities of arc induced shockwave with different voltages (frequency of 1 kHz).

The velocity measurement of the induced shockwave has also been conducted. Figure 6 shows the velocity evolution when the discharge voltage varies from 13 kV to 17 kV at a fixed pulse frequency of 1 kHz. Figure 7 shows the velocity variation with the frequency increasing from 400 Hz to 2000 Hz at a voltage of 15 kV. It should be noted that all the velocities are time averaged for the past 10 μs. The similarity can be easily found between the two figures. At the beginning, the velocity of the shockwave is as high as over 410 m/s, however, it decreases to 380 m/s in the following 10 μs, gradually falls to about 340 m/s in the next 40 μs, and becomes stable there, which means that the shockwave has become weaker and transmitted sonically. Actually, there is no definite rules stating how the discharge voltage or the pulse frequency influence the propagation, at every test point of certain voltage and frequency, the velocities distribute closely to each other. The reason why the shockwave velocity does not change with the increase of the discharge voltage may be that once the geometry of the actuator is designed, the breakdown voltage is fixed, as long as the voltage applied between the electrodes is higher than the breakdown voltage, the arc will be created. From this perspective, there is no big difference whether the voltage is 13 kV or 17 kV. When it comes to the unchanged velocity under all testing frequencies, even at the frequency of 2 kHz, the interval between two discharges is nearly 500 μs, compared with the single pulse width of 6 μs, it is long enough for the heat transformation between the arc channel and the unheated air. So every pulse can be considered independent and generated in the same environment.

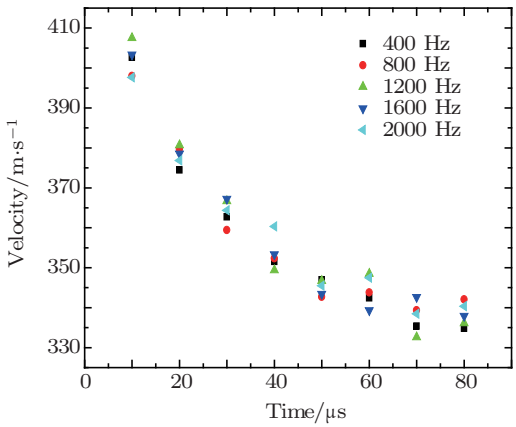


Fig. 7. (color online) Velocities of arc induced shockwave with different frequencies (voltage of 15 kV).

3. Numerical model and simulation

In order to better understand the mechanism and the characteristics of the arc induced shockwave, numerical investigations have also been carried out. After the modeling of the arc plasma, the commercial computational fluid dynamics flow solver Ansys CFX is adopted for calculation. A two-dimensional computational mesh is created using the ICEM-CFD grid generator.

3.1. Analytical model

The model of arc plasma has been developed using the energy equation applied to the control volume shown in Fig. 8. As shown above, Q_0 represents the total heat added into the control volume, while Q' represents the heat lost from the control volume through the control surface. The energy equation of the control volume can be written as follows:

$$\iiint_V \dot{q}\rho \,\mathrm{d}V - \iint_S \dot{q}' \,\mathrm{d}s - \iint_S \boldsymbol{PU}\cdot \mathrm{d}\boldsymbol{S} = \iiint_V \frac{\partial}{\partial t}\left[\rho\left(e+\frac{U^2}{2}\right)\right]\mathrm{d}V$$

$$+\oiint_S \rho\left(e+\frac{U^2}{2}\right)\boldsymbol{U}\cdot \mathrm{d}\boldsymbol{S}. \tag{1}$$

In the above equation, $\iiint_V \dot{q}\rho\,\mathrm{d}V$ represents the heat added into the control volume and $\oiint_S \dot{q}'\,\mathrm{d}s$ represents the heat lost from the control volume through the control surface. By making the assumption of a two-dimensional situation in the control volume, equation (1) can be simplified as

$$\frac{\mathrm{d}}{\mathrm{d}t}(\rho eV) = \dot{Q} - \dot{Q}' A_{\mathrm{SURFACE}} - \dot{m}h_{\mathrm{t}}, \tag{2}$$

where ρ is the gas density, e is the internal energy, $\dot{Q}$ is the energy depositing rate, $\dot{Q}'$ is the energy losing rate through the control surface, A_{SURFACE} is the area of the internal surface, $\dot{m}$ is the out mass flow rate from the control volume, and h_{t} is the total enthalpy flowing out of the control volume.

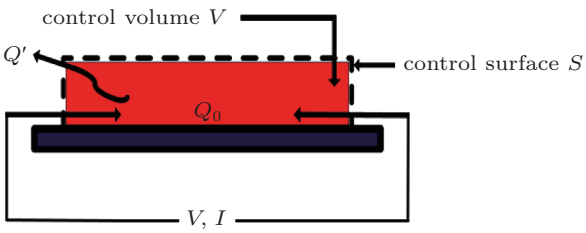


Fig. 8. Arc plasma control volume.

As shown in Figs. 2 and 3, the current duration is utmost 7 μs, while the power lasts even shorter (6 μs), as the heating process is ultrafast. Compared with the deposited energy $\dot{Q}$, the energy lost during this short period of time is quite tiny. Similarly, the out mass flow rate $\dot{m}$ is also vary small. So the heat transfer $\dot{Q}'A_{\mathrm{SURFACE}}$ and out flowing $\dot{m}h_{\mathrm{t}}$ can be ignored, and equation (2) is simplified as

$$\frac{\mathrm{d}}{\mathrm{d}t}(\rho eV) = \dot{Q}. \tag{3}$$

Here $\dot{Q}$ is a function of time, also written as $\dot{Q}(t)$, it represents the energy deposition rate into the arc channel, which is another expression of energy. After being added into the Navier–Stokes equations as a source term, the parameters like pressure can be acquired through solving the equations. Besides, $\dot{Q}$ is also related to the power plot acquired in the experiment.

3.2. Grid generation

The two-dimensional computational mesh shown in Fig. 9 is generated by the ICEM-CFD grid generation package. The mesh consists of 207912 total elements. A rudimentary grid sensitivity study including both a finer and coarser grid has also been carried out. The minimum difference of the shockwave velocity is less than 2%. Three domains are divided in the whole mesh, the air domain simulates the open and quiescent air in which the shockwave propagates, the arc domain is a newly-created subdomain which is defined as the source term, the ceramic holder of the electrodes is designed with a heat-transmitting coefficient of 0.85×10^3 J/Kg·K. It is helpful to explore the influence of the heat transfer between the heated air and the ceramic wall. Based on the Schlieren images, the cross section of the arc domain is defined to be 8 mm×2 mm. In order to acquire the changing rules of the shockwave velocity, the height and width of the air domain are set to be 20 mm and 38 mm, respectively.

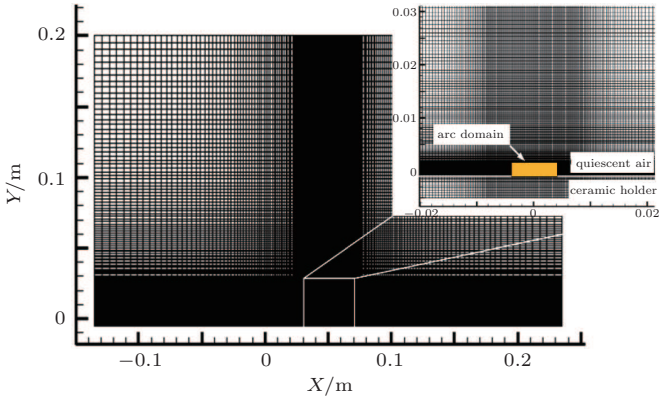


Fig. 9. Computational mesh generated by ICEM-CFD.

3.3. Source term and basic settings

In software-level computations, the thermal source term is usually marked as a rectangular or round area with a steady temperature, and the magnitude is estimated through an experimental non-intrusive measurement. Here in this paper, the source term of the arc plasma is set in the form of instantaneous power density, which is acquired from the V–I plot. With the time-resolved power plot, the influence of the energy depositing rate is expected to be revealed, the heating process will also be simulated and more precisely described.

Figure 10 shows the comparison of instantaneous power between simplified plot and experiment, the upper curve is a replot of Fig. 3. With the location of the inflection point, the form of power plot can be roughly copied and then used in the numerical simulation. As mentioned above, with the power and the volume of the heated area, the power density can be acquired, which is adopted as the thermal source term and added in to the energy equation. Through solving it, the temperature and pressure are finally calculated.

The ideal gas is chosen as the working material in the air domain, the environmental parameters include a temperature of 288 K, a pressure of 96610 Pa, and a density of 1.19 Kg/m^3. As there is no remarkable effect of repetitive discharge, only the single pulse discharge is simulated. In the center of the arc domain, a point (coordinates $X\times Y$ of 0 mm×1 mm) is set to monitor the core parameters of the arc plasma. During the

calculation of the power density, the three-dimensional size of the arc domain is assumed to be 8 mm×2 mm×4.5 mm. As seen from Fig. 10, with the peak power of 201.09 kW, the peak power density is 2.793×10^{12} W/m^3. To investigate the influence of the discharge power, besides the baseline peak power density, other different values are also selected. All the simulation parameters are listed in Table 1. In order to be consistent with the experimental conditions, the pressure in the simulation is determined according to the altitude of the place where the experiment has been conducted. So, with the altitude of 400 m, the pressure is 96610 Pa. It should be noted that in the numerical simulation, the changing time step is applied according to different phases. During the heating process, the time step is minimized to be 1 ns, while the biggest time step is up to 2 μs in shockwave propagation. The total time of simulation is 500 μs in all cases.

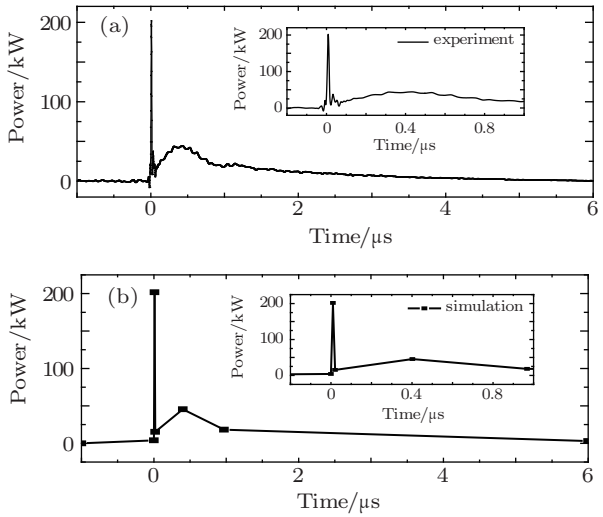


Fig. 10. Comparison of power plot between (a) experiment and (b) simulation; enlarged plots are shown in the insets.

Table 1. Boundary conditions and peak power densities.

Global parameters	Peak power density/10^{12} W·m^{-3}
Pressure = 96610 Pa	1.4
Temperature = 288 K	2.1
Density = 1.19 Kg/m^3	2.8 (baseline)
Cross section of arc domain = 8 mm×2 mm	3.5
	4.2

3.4. Results

3.4.1. Validation of numerical model

After being established, the numerical model is validated with the experiment results at the frequency of 1 kHz and voltage of 15 kV, the simplified power plot (see Fig. 10) is taken as the source term. Figure 11 shows the pressure variation during the shockwave movement within 80 μs, basically it coincides with the experiment result. The locations of pressure peaks at different simulating moments are shown in Fig. 12. At 10 μs, the peak value of the pressure is about 6 mm above the actuator wall, which indicates the passing by of the induced shockwave. During the propagation, both the peak value and the velocity of the shockwave are decreasing. Figure 13 shows the velocity comparison between simulation and experiment. At the first 30 μs, the simulated shockwave velocity is faster than the experimental value, after that, the result shows an agreement with each other, both of them stay at about 340 m/s.

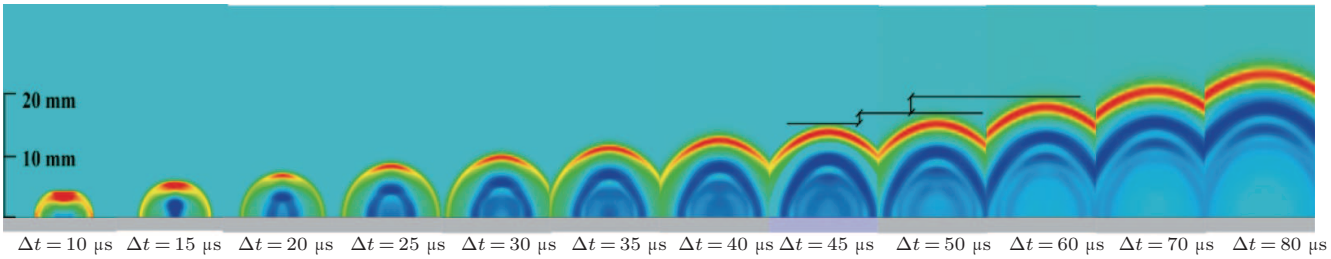


Fig. 11. (color online) Contours of pressure variation during shockwave propagation with power density of 2.8×10^{12} W/m^3.

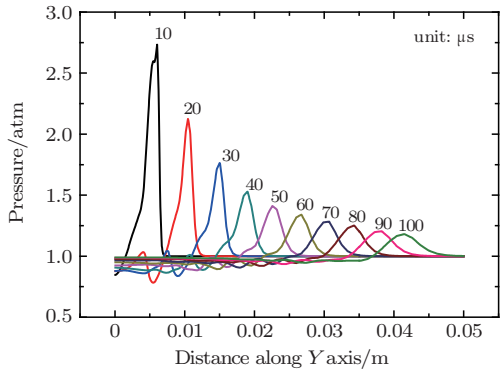


Fig. 12. (color online) Pressure distributions along the Y axis at different moments.

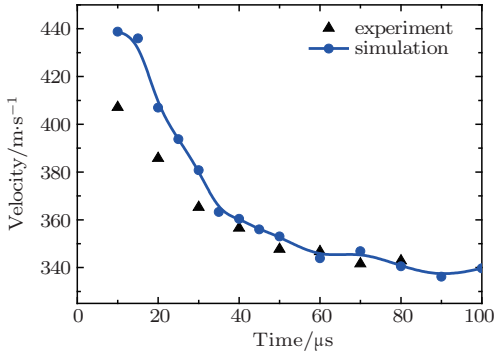


Fig. 13. (color online) Comparison of shockwave velocities between experiment and simulation.

3.4.2. Arc domain after discharge

In the core of the arc domain, the variations of pressure and temperature are recorded. Figure 14 shows the pressure development with different discharge power densities. With the maximum power density of 4.2×10^{12} W/m^3, the pressure rise reaches over 5 times of that before discharge, while given the minimum input power density of 1.4×10^{12} W/m^3, the pressure only rises about 2.5 times of that before heating. Also it is found that with a higher input power density, the pressure will reach the peak value faster. As Fig. 15 shows, when more energy is deposited into the arc domain, the core temperature rises to over 1600 K. From the viewpoint of a heating mechanism, it is more ideal to acquire a strong actuation for the high speed flow control.

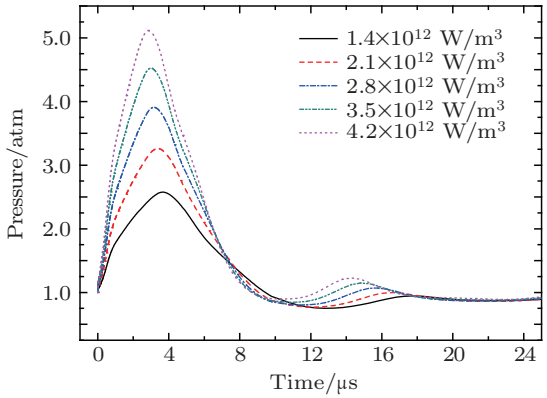


Fig. 14. (color online) Pressure curves with different discharge power densities.

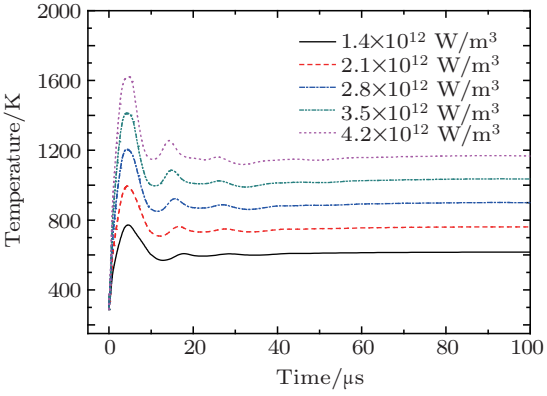


Fig. 15. (color online) Temperature curves with different discharge power densities.

3.4.3. Velocity of arc induced shockwave

The influence of the discharge power density (representing the heating strength) on the shockwave velocity is investigated, too. Five curves of velocity according to different power densities are shown in Fig. 16. It is easy to find that when a higher power density is input, the shockwave will move faster. At 4.2×10^{12} W/m^3, the highest velocity acquired is up to 468 m/s. During the first 30 μs of the shockwave movement, the variation of velocity is more obvious, and then it becomes weaker, especially after 80 μs. At that time, the shockwave may have already changed into a weak disturbance and travels at the sound speed. Besides, with the increase of the input power density, the induced shockwave can endure and exist longer. For instance, at 60 μs, with the power of 1.4×10^{12} W/m^3, the shockwave has already been moving sonically, while under the power of 4.2×10^{12} W/m^3, it still moves at about 390 m/s. So, with more energy deposited, it is quite possible to create a stronger and longer-enduring disturbance into the open air.

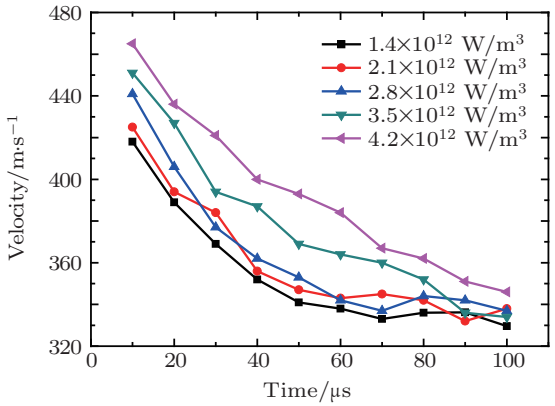


Fig. 16. (color online) Velocities of induced shockwave under different discharge power densities.

4. Discussion

As mentioned above, with rapid heating caused by arc discharge, the temperature and the pressure of the arc channel will sharply rise in a very short time. The process is somewhat like an explosion, and then the shockwave origins from the interface between the arc area and the undisturbed air. During its upward movement, the temperature and the pressure will keep decreasing owing to heat transmitting and air friction. About 60 μs later, the shockwave has changed to a weak disturbance and travels sonically.

Such a tendency can also be found in the simulation, the difference is that the calculated velocity is larger than the experiment one at the same moment. To explain this, it should be noted that between the anode and the cathode, the distribution of the voltage drop is not uniform. Near the cathode there is a very small area where much positive charge is gathered, usually the current density there is much higher than that in other regions. This means that the heating process will be stronger and brings a sharper rise of temperature and pressure. However, in the simulation, the whole arc domain is designed to be uniform with the same input power density, although the peak value is precisely reflected in the numerical model, it still may enlarge the input power and make the shockwave move faster. On the other hand, because of the higher temperature, there would be a bigger temperature gradient with which the heat transmission would be quicker. So it is no wonder that

the simulation matches the experiment results after tens of microseconds.

At last, some efforts have been made to research the influence of the heat transfer between the electrodes and the ceramic holder. Unfortunately, at the highest power density of 4.2×10^{12} W/m^3, the temperature of the ceramic hardly rises (only about 0.1 K) in 500 μs. Probably it is too short to transfer heat between the air and the ceramic plate. It is quite reasonable to believe that the temperature will keep rising under repetitive discharges, however how it affects the shockwave generation is still unknown.

5. Conclusion and outlook

The characteristic of the surface arc plasma induced shockwave has been investigated both experimentally and numerically. Based on the Schlieren measurement, it is found that when the discharge voltage increases from 13 kV to 17 kV and the frequency varies between 400 Hz and 2000 Hz, the peak value of the shockwave velocity does not change remarkably, but keeps stable around 410 m/s. During its propagation, the shockwave is weakened and finally becomes a disturbance which travels sonically. The simulation results show a similar trend, the difference is that within 30 μs after discharge, the velocity is bigger than the measured one. Enlarging the input power will lead to the rise of temperature and pressure in the arc domain, thus the shockwave velocity can be increased.

Future work should focus on the interaction between the induced shockwave and the high speed flow. Small-scaled supersonic wind tunnel tests should be conducted to explain how the shockwave influences the flow field. Besides, some adjustments are necessary to improve the numerical model in order to optimize the parameters and the structure of the actuator.

References

[1] Bletzinger P, Ganguly B N, Wie D V and Garscadden A 2005 *J. Phys. D: Appl. Phys.* **38** R33

[2] Corke T C and Post M L 2005 43rd *AIAA Aerospace Sciences Meeting and Exhibit,* January 10–13, 2005 Reno, USA

[3] Sanders B, DeBlauw B, Elliott G, Dutton C and Glumac N 2012 50th *AIAA Aerospace Sciences Meeting including the New Horizons Forum and Aerospace Exposition,* January 9–12, 2012 Nashville, USA

[4] Shin J and Mahadevan S 2011 *Aerospace Sci. Tech.* **15** 18

[5] Leonov S B, Yarantsev D A, Gromov V G and Kuriachy A P 2005 43rd*AIAA Aerospace Sciences Meeting and Exhibit,* January 10–13, 2005 Reno, USA

[6] Leonov S B and Yarantsev D A 2008 *J. Propul. Power* **24** 1168

[7] Leonov S B and Yarantsev D A 2008 *Fluid Dynamics* **43** 945

[8] Leonov S B and Yarantsev D A 2008 *IEEE Trans. Plasma Sci.* **36** 978

[9] Leonov S B and Yarantsev D A 2007 *Plasma Sources Sci. Technol.* **16** 132

[10] Hahn C, Fischer M K and Samimy M 2011 *Exp. Fluids* **51** 1591

[11] Samimy M, Kim J H, Kastner J, Adamovich I and Utkin Y 2007 *J. Fluid Mech.* **578** 305

[12] Shneider M N and Macheret S O 2006 *J. Propul. Power* **22** 490

[13] Shneider M N, Macheret S O and Miles R B 2007 *AIAA J.* **45** 2157

[14] Shang J S, Chang C L and Surzhikov S T 2007 *AIAA J.* **45** 2710

[15] Shang J S 2008 *J. Spacecraft Rockets* **45** 1213

[16] Kuo S P, Rubinraut M, Popovic S and Bivolaru D 2006 *IEEE Trans. Plasma Sci.* **34** 2537

[17] Kuo S P and Kuo S S 2006 *Phys. Plasmas* **13** 033505

[18] Ni G H, Meng Y D, Cheng C and Lan Y 2010 *Chin. Phys. Lett.* **27** 055203

[19] Pan W X, Li T, Meng X, Chen X and Wu C K 2005 *Chin. Phys. Lett.* **22** 2895

[20] Xu D A, Lacoste D A, Rusterholtz D L, Elias P Q, Stancu G D and Laux C O 2011 *Appl. Phys. Lett.* **99** 121502

[21] Gaitonde D V 2012 *J. Propul. Power* **28** 281

[22] Yan H and Gaitonde D V 2011 *Shock Waves* **21** 411